

Fiber Fabrication and Characterization¹

1 Introduction

The fabrication of an optical-fiber cable consists of the manufacturing fabrication of the glass master (called a “preform”); the drawing of the fiber itself; and the bundling of the fiber, strength members, filler yarns, and other components into a cable. We will consider first the fabrication and testing of the optical fibers and then the concerns in assembling an optical cable. The fabrication of the fiber can be done with either of two classes of techniques, those using high-melting-temperature glasses involving vapor deposition of the glass material and those using low-melting-temperature glasses that make the fiber directly from the melted glass. The fiber is drawn from the stock material by a pulling machine under constant tension and reeled on a spool. Following testing and characterization of the fiber, it is incorporated into an optical cable having the desired environmental protective features.

2 Glass

Glass is an amorphous crystalline material that has a wide range of viscosity values as a function of temperature. Unlike ordinary crystals that have a regular periodic lattice of atoms and a well defined melting temperature, glass is an irregular suspension of molecules and no well defined melting temperature. Instead, as the temperature increases, the viscosity decreases. Since there is not an abrupt change in the phase of the material, the *melting temperature* becomes a matter of definition rather than a physical observable. The *softening temperature* occurs at a viscosity value of 3.16×10^7 poise and the *working temperature* at a viscosity value of 1.0×10^4 poise.

For fiber-optics purposes, there are two general kinds of glass. The majority of fibers are made of *fused silica* (SiO_2) to which dopant materials are added to change the index of refraction. Some fibers are made of softening *multicomponent glasses* [1], i.e., they are made up of a variety of components. Examples of the latter include sodium borosilicate ($\text{Na}_2\text{O}-\text{B}_2\text{O}_3-\text{SiO}_2$) and soda lime silicate ($\text{Na}_2\text{O}-\text{CaO}-\text{SiO}_2$). The working temperature for the silica-based glasses is in the vicinity of 1800 C, while the working temperature of the compound glasses is 900 C. The role of dopants in silica glass is shown in Fig. 1 on the following page, which plots the index of refraction of the glass vs. the concentration of dopant material. Here we see that the addition of GeO_2 or P_2O_5 raises the index, while the addition of B_2O_3 lowers the index. Hence, the addition of the proper element

¹From John Powers, *An Introduction to Fiber Optic Systems*, ©Richard D. Irwin, Inc., and Aksen Associates, Inc., Burr Ridge IL, 1993.

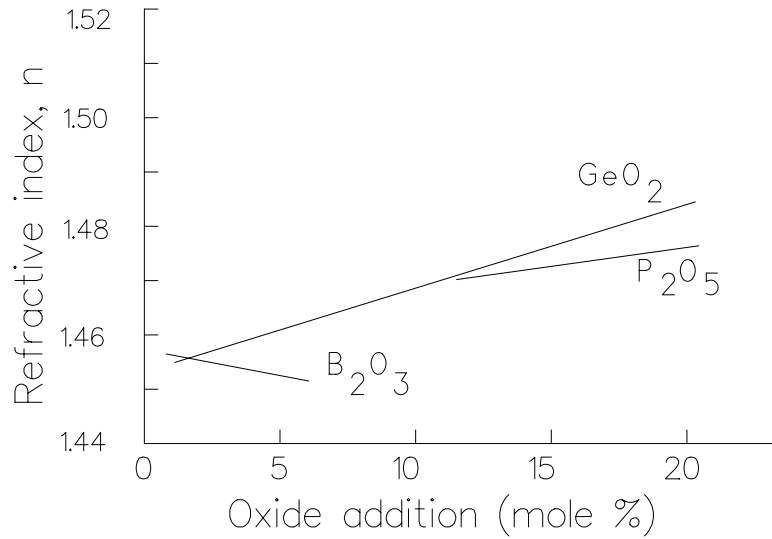


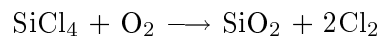
Figure 1: Refractive index of silica-based glass vs. concentration of dopant.

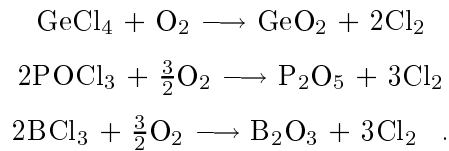
in the right proportion can raise or lower the refractive index to the desired value. Note from the figure that we can raise the index by a Δ of 1.4% and lower it by only 0.2%. Because of the wide difference in working temperatures for the two types of glass, there have evolved two fundamentally different techniques in making fibers, one involving the use of *preforms* and another growing the fibers directly from melted glass.

3 Preform Fabrication [2, 3]

Fabrication of fibers using high-melting-temperature silica glass utilizes preforms which are cylinders of glass, tens of millimeters in diameter, with an index of refraction profile that is an enlarged replica of the desired profile (i.e., the core area and cladding area are in the same proportion that they will be in the fiber). Both graded-index and step-index fibers can be made by this technique. The preform serves as the stock material for the fiber drawing process and should be as long as possible to maximize the amount of fiber that can be drawn from a single preform. The preforms for the silica-based glass are usually made by a *vapor phase process*.

These techniques start with a high-purity silica-base stock. Impurities and glass are then deposited to change the index of refraction in a prescribed fashion. Typically the impurities and glass are introduced as a vapor of chloride combinations that are oxidized in a flame to produce the desired dopant products and that combine with silica vapor for the deposition process. Typical reactions include





The first products are the desired glass and dopants; the chlorine by-products are extracted in the exhaust. Hydrogen-based flames can also be used for hydrolysis, but the resulting water product must subsequently be removed by careful drying to avoid excess losses in the glass due to the hydroxyl ions.

The glassy product of the vapors is called *soot* and is deposited on the surface of a glass or graphite rod (called the *bait rod*) in the form of a porous material. This porous soot is reduced to smooth clear glass by heating it to approximately 1500 C in a process called *sintering*. The radial dimension is built up layer by layer in this fashion with 100 layers typically being deposited. For a step-index fiber, the concentration of impurity is maintained constant in all layers. For graded-index fibers, the concentration is gradually changed from layer to layer to build up a stepwise approximation to the desired index profile.

3.1 MCVD Process [3–7]

One common method of fabricating the preform uses the *modified chemical vapor deposition (MCVD) process*, developed by Bell Laboratories. This process is called an *inside process*, since the doped glass is deposited on the inside surface of a hollow rod. (This class of inside processes is called the *inside vapor phase oxidation [IVPO] process*.) The IVPO process has the advantage of confining the interaction region, thereby lowering the chances of contamination by outside impurities. The process is illustrated in Fig. 2 on the next page.

The gaseous vapors of the glass and impurities enter the hollow cylinder as hot gases and are attracted to the cool walls of the tube. The tube rotates to preserve the cylindrical symmetry of the deposition. A torch traverses the length of the tube to heat the deposition and sinter the material into smooth glass. Since only the region near the torch is heated, this process is called *zone sintering*.

A variation of the MCVD technique uses an RF-generated plasma inside the tube to increase the soot deposition rate while retaining the outside torch to sinter the glass. It is called *modified plasma chemical vapor deposition (MPCVD)* [8]. A variation on this variation uses a plasma for both internal and external heating of the tube and is called the *Philips process* after the company developing the technique.

After the deposition process is completed, the entire tube is heated to high temperatures, thereby collapsing the tube and eliminating the central hole. This solid rod is the preform that is then used in the drawing machine to produce the fiber. Primary disadvantages center around the high purity tube stock required for the process. Various techniques are under investigation to provide a low cost, reproducible means of producing

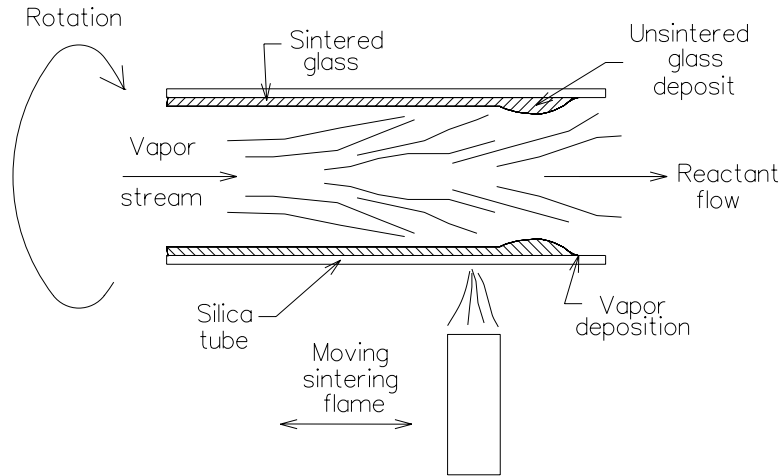


Figure 2: Diagram of the MCVD process.

the tube stock. Another minor disadvantage is the relatively slow rate of soot deposition in the tube. The development of the faster depositing plasma process was driven by this problem.

3.2 Outside Vapor Deposition Process [3, 9, 10]

The *outside vapor phase oxidation (OVPO)* deposition process occurs on the outside surface of the host material. The process is subdivided into two types, depending on whether the new material is deposited radially (laterally) or longitudinally on the end of the host. Again, the deposition process is based on the deposition of soot from hot gases containing the glass material and the dopants.

3.2.1 OVPO-Lateral Deposition

The lateral deposition process (Fig. 3 on the facing page), developed by Corning Glass Works, deposits the soot on a removable host material called a *bait rod*. This rod is typically made of graphite, fused silica, or ceramic. The rod again rotates to assure symmetry. The layers are built up in unsintered form until typically 200 layers have been deposited. After the soot deposition process, the inner bait rod is removed and the deposited material is zone sintered to reduce its radius and to form the smooth glass. Note that both the core and cladding material are deposited in this case, unlike the MCVD deposition where the host tube became the cladding material. The larger number of layers in the OVPO process allows more precise control over the refractive index profile. High bandwidth-distance fibers result from this control. The resulting preforms are also longer, allowing more fiber to be drawn (up to 10 km of 125 μm

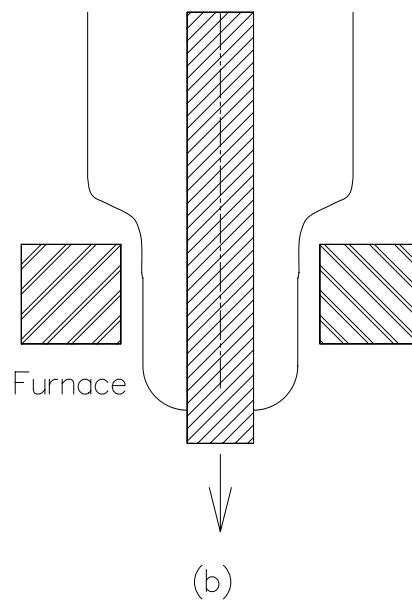
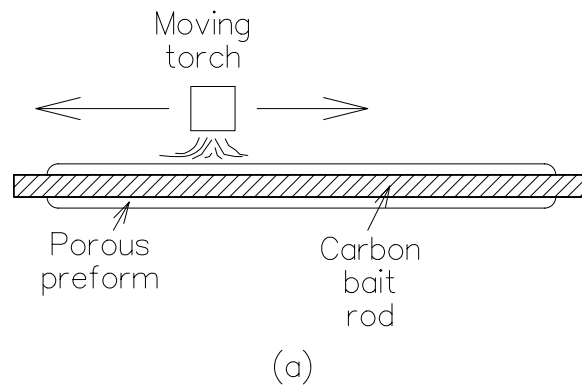


Figure 3: OVPO process. (a) Lateral deposition. (b) Sintering process.

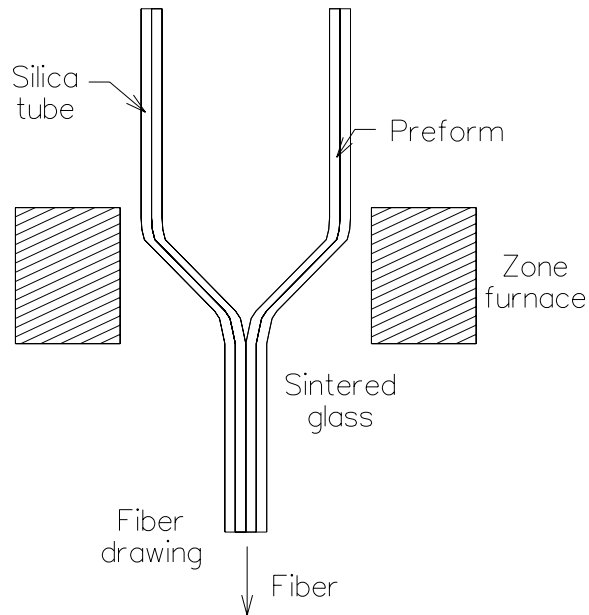


Figure 4: Preform hole removal during drawing of fiber.

diameter fiber). One difficulty [3] has been the breakage of the glass blanks due to localized stresses where the bait rod has been removed. Another problem has been the presence of high concentrations of hydroxyl ions as a result of the flame burning. This can be removed by careful drying with gaseous chlorine during the sintering process. As shown in Fig. 4, the hole in the preform is removed during the melting process associated with the drawing process (although a dip in the index of refraction along the central axis due to the outward diffusion of the impurities in the heating process is left as an artifact).

3.2.2 Vapor Axial Deposition Process [3, 11–13]

The *vapor axial deposition (VAD) process*, developed by Nippon Telephone and Telegraph, simultaneously deposits the core and cladding glass from flames on the end of a rotating fused-silica bait rod. Shown in Fig. 5 on the facing page, the material is sintered as the rotating rod is drawn through a furnace. Since the growth is continuous, very long preforms can be made from this technique; in fact, preforms yielding in excess of 25 km of fiber have been made. The method also lacks a center hole and, through the combination of the deposition and sintering process, can minimize the contamination problem. This technique has also been used to grow core material that is then placed inside tubes of cladding material (called the *rod-in-the-tube technique*) or that is plastic-clad to produce the preform for fiber drawing. One major problem with this technique

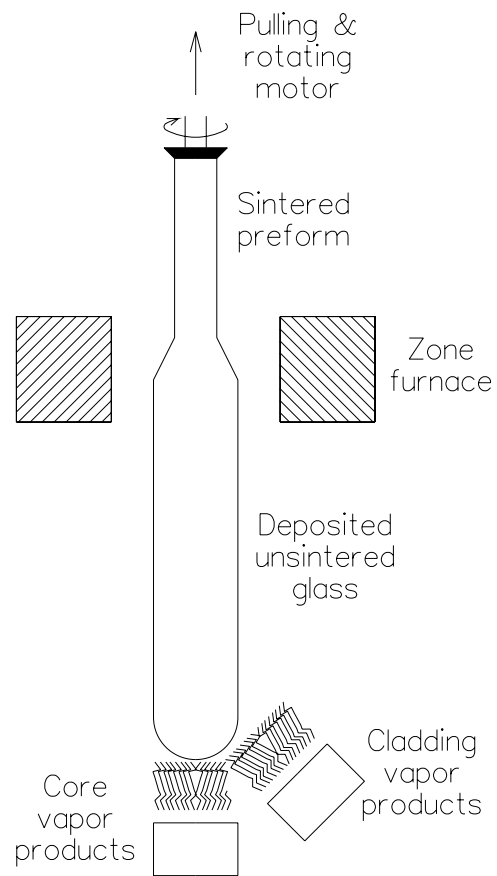


Figure 5: Vapor axial deposition.

is the precision of control of the refractive index variation. Also, the deposition rate of the material (typically 0.5 g/min) is low compared with other techniques.

4 Double-Crucible Technique [1, 3]

For low-melting-temperature compound glasses, a preform is not used. Instead the stock material is purified and grown into rods from seed glass. This seed glass is melted and used in the fiber growing process, as shown in Fig. 6 on the next page. Here two concentric platinum heating chambers contain the liquefied glass for the core and cladding. The fiber is drawn from two concentric orifices at the outlet of the crucibles. The feed stock is continuously fed into the crucibles to replenish the supply of glass. Graded-index fibers are made in the double-crucible process by allowing the molten cladding glass to contact the core glass over a relatively long length before the fiber leaves the crucibles. Over this length, diffusion of ions occurs, causing a gradient and, hence, a variation in the index of refraction. The advantages [3] of the double-crucible process include the abilities draw long fibers, to produce fibers with high numeric apertures, and to achieve low cost. Disadvantages include the requirement for extreme cleanliness in the crucibles and orifices and a relatively low bandwidth-distance product (typically <1 GHz·km) [3]. For medium-performance fibers, however, the low production costs ensure a future role for this technique.

5 Fiber Drawing [14–17]

Once a preform has been made by one of the vapor-deposition techniques, the fiber is then drawn in a *drawing engine* or *drawing machine*. A block diagram of such a machine is shown in Fig. 7 on page 10. The heat source is typically a graphite or tungsten furnace or a zirconia induction furnace. Uniformity of heating, lack of contaminants, and stable temperatures are the primary requirements of the heating source. When heated, the end of the preform will become molten and neck down into a smaller cross-section, but the glass will preserve the relative core/cladding size relation established in the fabrication of the preform. Since most of the fiber properties (losses, delay, etc.) are sensitive to small changes in the fiber diameter, a sensitive diameter sensor is required. Traditionally a good fiber requires less than $\pm 2\%$ variation in its diameter. Control of the diameter is through an active mechanism that senses the fiber diameter and then adjusts the speed of the drawing operation accordingly. (See problems at the end of the chapter.) Various optical techniques using scanned lasers, scattered light, shadowgrams, and other methods have been developed to achieve the required dimensional sensitivity. In the drawing process, fast drawing velocities cause thin fibers, thereby allowing the feedback control system to maintain the fiber size.

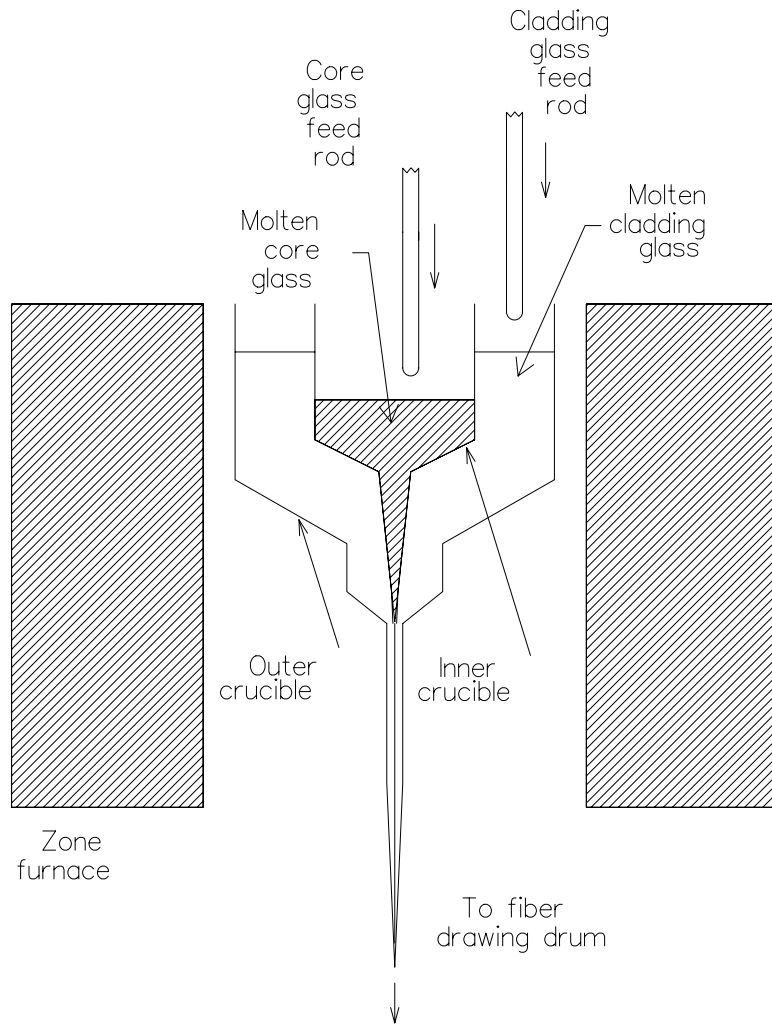


Figure 6: Double-crucible process.

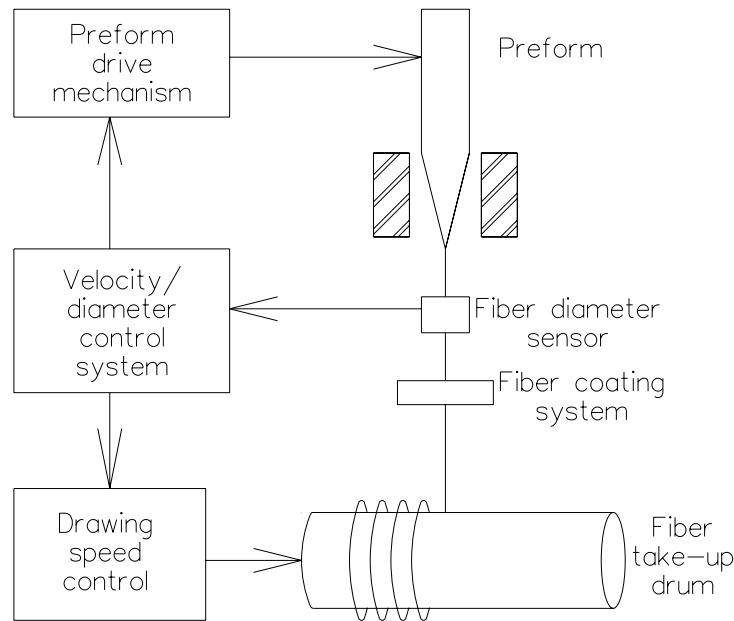


Figure 7: Fiber drawing machine.

6 Fiber Coating [15, 18]

After drawing the fiber, it is important to protect the outside surface of the fiber from the environment immediately. This is necessary because any defect or flaws in the outside surface of the cladding will have deleterious effects on the strength of the fiber. The coatings used must be fast drying and provide complete protection from the spooling process. Typically, one of three coatings is used: ultraviolet curable epoxies, lacquers, and thermally cured materials such as silicone. Each coating requires a curing device surrounding the fiber, either an ultraviolet light or a small oven. Figure 8 on the next page illustrates the application of the liquid coating material through the use of a coating cup.

6.1 Hermetic-Coated Fibers [7, 19–23]

Several application areas for fiber optics require combinations of high strength [19, 23, 24] and long life. Table 1 on the facing page contains a representative list of some of these applications. (Regular fiber strength for ordinary telecommunications applications has a proof strength of about 180 kpsi. The strength drops to 100 kpsi in 10 days, 80 kpsi after 100 days, 65 kpsi after three years, and an estimated 45 kpsi after 30 years.) Fiber coatings also prolong the shelf-life of the fiber by protecting it from the environment. Hermetic coatings may prolong the life from an estimated 15 years to 25-30 years.

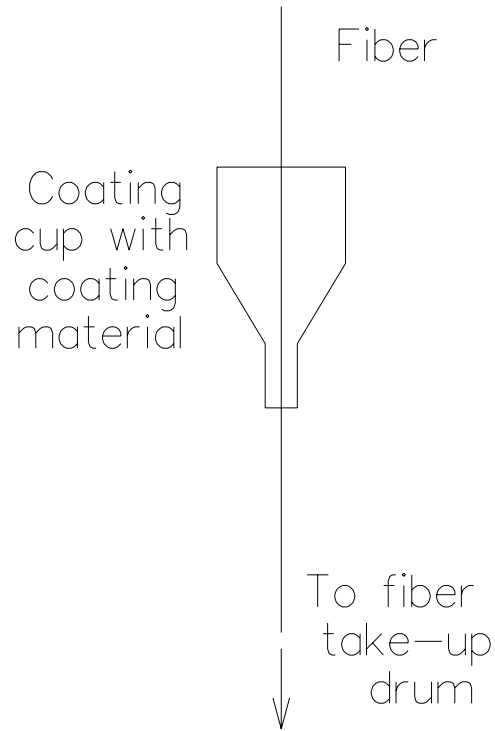


Figure 8: Coating process with coating cup.

Application	Operating conditions			Lifetime
	Pressure	Temperature	Strain	
Oil-well logging	20 kpsi	200C	3% 300 kpsi	4000 hrs
Underseas cable	2-10 kpsi	5C to 25C	1% 100 kpsi	25-30 yrs
Missile tethers	1 atm	-55C to 125C	0.5% to 1% 50-100 kpsi	10 yrs
Chemical sensors	1 atm	Depends on application	0.5% to 1% 50-100 kpsi	10 yrs 10 yrs
Standard telcomm	1 atm	-25C to 70C	0.5% to 1% 50-100 kpsi	25-30 yrs 10 yrs

Table 1: Typical high-strength fiber applications (After J. Kreidl, *Lightwave*, vol. 4, no. 1, p. 1, November, 1987.)

Coating	Thickness (μm)	Median strength (kpsi)
Aluminum	15–20	529
Titanium oxide	0–5	500
Tin oxide	0.01–0.035	620
Aluminum oxide	0.02–0.04	435
Silicon oxynitride	0.02–0.04	200–300
Silicon carbide	0.02–0.06	500
Titanium carbide	0.025–0.05	400–500
Carbon by CVD	0.02–0.025	600–650
Carbon by plasma	0.020	730
Anhydrous CH	0.025–0.050	500–600

Table 2: Typical hermetic coatings (After J. Kreidl, *Lightwave*, vol. 4, no. 1, p. 1, November, 1987.)

Hermetic coatings are a microlayer of inorganic material around the outer circumference of a fiber with a thickness of no more than a few micrometers. The coatings can be applied to high-strength or medium-strength fibers, increasing the lifetime of the coated fiber and improving yields (since fiber that fails to meet any strength tests is discarded). The coating is required to be impermeable, to not allow pinhole defects, and to have thermal expansion properties that match the glass fiber. Chemical vapor deposition techniques are preferred for coating silica fibers. The primary advantage of the hermetic-coated fiber is its higher resistance to stress fatigue, hydrogen permeation, and corrosive chemicals. Additionally, coated fibers using titanium carbide can be soldered or bonded to ensure waterproof operation, allowing the entire fiber system to be hermetically sealed (since sources and receivers are already available in hermetically sealed packages). Efforts are also underway to develop techniques for splicing these fibers while retaining the hermetic seal [25].

Several fiber coatings on silica fibers are under investigation, as seen in Table 2. Various coatings are being studied to find an optimum combination of properties and to provide patent protection for the developer.

7 Polymer-Clad Silica (PCS) Fibers

A third type of fiber is made by heating a rod of purified fused silica and drawing a fiber. This fiber is immediately coated with plastic or silicone and covered by an extruded protective jacket. Here the silica serves as the core material and the coating is the cladding. Such fibers typically have losses on the order of 10 dB/km or more, are very inexpensive to make, and usually have a fairly large core.

8 Preform and Fiber-Profile Characterization [26–34]

Preform characterization is done to predict the quality of the resulting fiber before drawing begins and to screen against unacceptable materials. The primary parameter to be measured in the preform or fiber is the index of refraction profile, $n(r)$, across the diameter of the glass. For the general case of a graded-index fiber, the preform profile is a scaled replica of the fiber profile and can be given by

$$n(r) = n_1 \sqrt{1 - 2\Delta \left(\frac{r}{a}\right)^g} \quad (\text{for } r < a), \quad (1)$$

where r is the radial coordinate, Δ is the relative index difference ($= [n_1 - n_2]/n_1$), and g is the exponent of the power law that determines the profile shaping. Neglecting material dispersion, the optimum value of the profile factor, g_{opt} , that maximizes the fiber bandwidth is given by repeated here as

$$g_{opt} = 2 - \frac{2n_1}{N_{g1}} \frac{\lambda}{\Delta} \frac{d\Delta}{d\lambda}. \quad (2)$$

To achieve the performance theoretically predicted for a fiber, the manufacturer must typically maintain the profile to within 1% of its optimal value [35]. Several effects in the fabrication process counter this attempt:

- As previously described, several fabrication techniques deposit the glass in layers, each with a slightly different index of refraction. Near the core center, the layers have proportionally greater thickness than the outer layers of the preform. In this region near the center, therefore, the index distribution will have ripples, due to the stepwise approximation to the desired profile.
- Another effect causing variation from the ideal index profile is a discontinuity in the index of refraction at the core-cladding interface. This effect is observed in some MCVD preforms.
- When the preform is made by heating and collapsing a tube with a center hole, some of the impurities of the innermost layer evaporate from the glass at the inner surface. This causes a depression in the index of refraction at the center of the preform, as illustrated by the profile of Fig. 9 on the following page.
- Occasionally the dopant atoms will clump together due to imperfections in the doping process or inhomogeneities in the soot. Such inhomogeneities tend to cause isolated regions that differ from the desired index profile. The bandwidth of the fiber is more sensitive to this effect when the imperfections are located near the core-cladding interface.

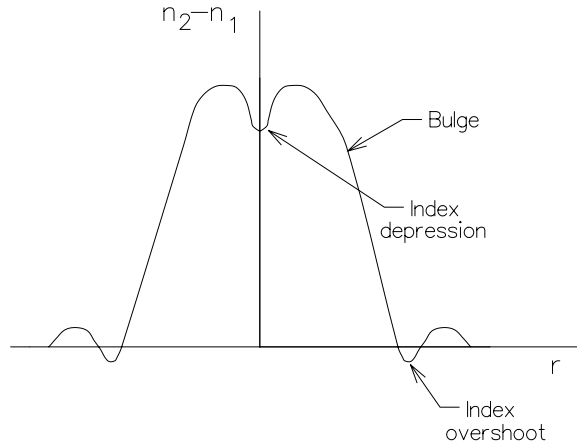


Figure 9: Typical refractive index profile.

- The refractive-index profile changes over the length of the preform due to variations in the geometry, temperature profile, and doping density.

Deviations from the ideal refractive-index profile, due to these mechanisms, typically cause an order of magnitude reduction in the experimentally observed bandwidth, compared to the predicted bandwidth in modern fibers.

8.1 Reflection Technique

The earliest profile techniques used the reflection coefficient to measure the profile. In this *reflection technique*, a light beam is focused on the end of a cutoff section of a preform (as in Fig. 10 on the next page) and the reflected power is measured as the focused beam scans radially. The reflected power is predicted to be

$$\frac{P_r(r)}{P_i} = \left(\frac{n(r) - 1}{n(r) + 1} \right)^2, \quad (3)$$

where P_r is the reflected power, P_i is the incident power, and $n(r)$ is the refractive index profile. Measurement of the reflected light power for a constant incident power allows calculation of the $n(r)$ (since $n(r)$ must be positive). The calculation is made easier by continuing the scanning out to the cladding region. Here, the reflectivity is given by

$$\frac{P_{r \text{ clad}}}{P_i} = \left(\frac{n_2 - 1}{n_2 + 1} \right)^2, \quad (4)$$

where n_2 is the refractive index of the cladding and $P_{r \text{ clad}}$ is the power reflected from the cladding region of the fiber. Taking the ratio of Eq. 3 to Eq. 4 and defining it as

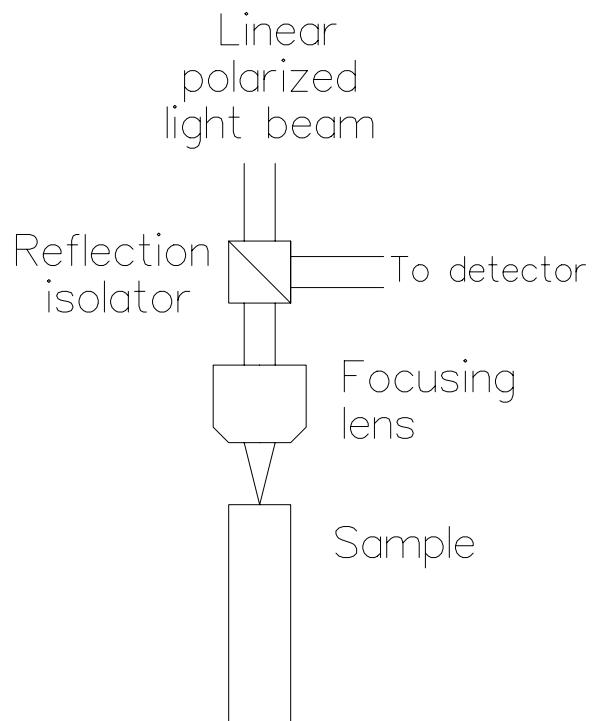


Figure 10: Reflection technique setup.

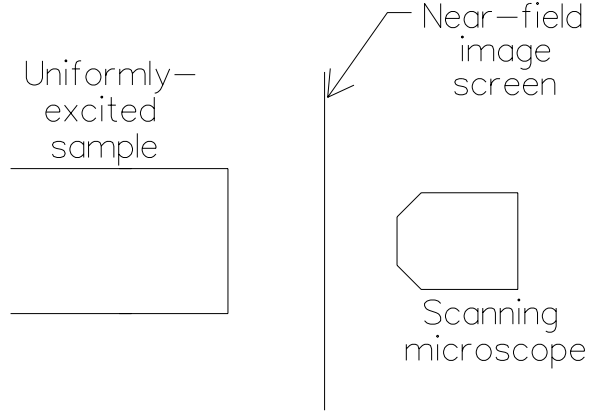


Figure 11: Geometry of the transmitted near-field technique.

$F(r)$, we have

$$F(r) = \frac{P_r(r)}{P_{r \text{ clad}}}. \quad (5)$$

From this definition of $F(r)$, we find that

$$n(r) - n_2 = \frac{(n_2^2 - 1)(\sqrt{F(r)} - 1)}{(n_2 + 1) - (n_2 - 1)\sqrt{F(r)}}. \quad (6)$$

The expected variations in reflectivity in an optical preform are fairly small. The system errors encountered in implementing the reflection technique are sufficiently large to give large errors. Surface contamination effects are also large enough to give errors in the measured reflectivity. In implementing this technique, linearly polarized light is used in combination with a quarter-wave plate (immediately in front of the glass surface) to remove undesirable reflections. Other techniques have generally surpassed the performance of the reflection technique.

8.2 Transmitted Near-Field Technique

The next technique, called the *transmitted near-field technique*, uses the properties of the light transmitted from the end of a fiber that has had all modes uniformly excited by the source. If one observes the pattern of light at a location close to the end of the fiber (as in Fig. 11), it closely resembles the refractive index profile of the fiber. Theory predicts that the relation between the power in the near-field pattern and the refractive index profile is [36, 37]

$$\frac{P(r)}{P(0)} = \frac{n^2(r) - n_2^2}{n^2(0) - n_2^2} \approx \frac{n(r) - n_2}{n(0) - n_2}, \quad (7)$$

where $P(r)$ is the power in the near-field at position r , $P(0)$ is the detected power at the center of the near field distribution, $n(r)$ is the refractive index profile, $n(0)$ is the refractive index at the center, and n_2 is the refractive index of the cladding. Hence,

$$n(r) - n_2 \approx \frac{(n(0) - n_2) P(r)}{P(0)}. \quad (8)$$

The source is usually a large incoherent illuminator that excites all of the fiber modes. A focused microscope is used to scan the pattern close to the end of the fiber (or preform).

8.3 Refracted Near-Field Technique [30]

The *refracted near-field technique* is used to characterize fiber index profiles. This technique is quite accurate and is free of the errors due to leaky waves that affect other transmission techniques. (The *leaky waves* are light waves with exponentially decaying tails that spread into the cladding. While such waves will eventually be attenuated for propagation over a long distance, they can carry energy quite far in some cases, causing errors in the measurement of the refractive index profile by techniques that measure the light transmitted through the fiber.)

The refracted near-field technique removes the effects of these waves by surrounding the fiber with an index-matching solution that matches the cladding index. Additionally, an opaque collar is placed around the fiber (as shown in Fig. 12 on the next page) to block a portion of the light that is coupled into the index-matching solution. The light power, coupled into the matching solution, that passes beyond the screen is captured on the detector and is measured. The fiber is excited by a focused spot of light that is scanned to different positions on the fiber end (with the aid of a microscope). If we let $P(r)$ be the total power at the receiver when the *input* spot is at position r , then Snell's law predicts

$$n_2 \sin \theta' = n(r) \sin \theta \quad (9)$$

and

$$n(r) \cos \theta = n_2 \cos \theta'' \quad (10)$$

Removing θ from these equations gives

$$n_2 \sin \theta' = \sqrt{n(r)^2 - n_2^2 + n_2^2 \sin^2 \theta''}. \quad (11)$$

The angle θ''_{min} is determined from the size of the collar, as seen in Fig. 12 on the following page. The angle θ'_{max} is determined by the microscope objective chosen to focus the illuminating light. It can be shown [30] then that

$$n(r) - n_2 = n_2 (\cos \theta''_{min}) (\cos \theta''_{min} - \cos \theta'_{max}) \left(\frac{P(a) - P(r)}{P(a)} \right), \quad (12)$$

where $P(a)$ is the power measured at the detector when the incident spot is focused on the cladding and $P(r)$ is the power on the detector when the *incident* spot is a distance r from the center.

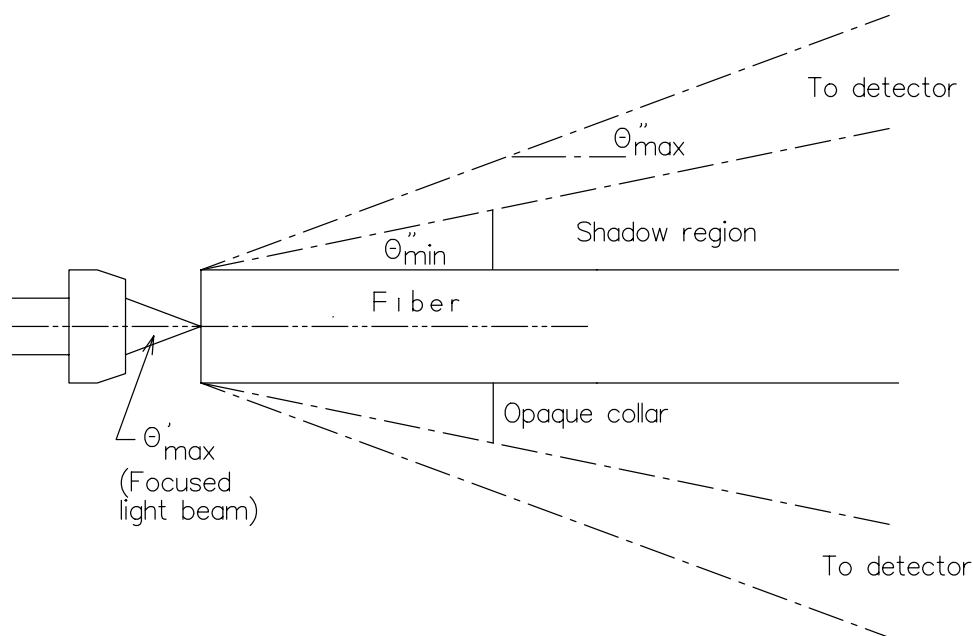


Figure 12: Refracted near-field technique.

8.4 Interference Techniques [1, 38]

Interference of coherent optical waves offers a way to measure small changes of phase induced by the refractive index profile. Two interference techniques have evolved.

The first is the *interferometric slab technique*, which uses a piece of excised fiber or preform (cut from the preform tip) that has been polished and prepared with parallel edges. The slab is placed in an interference microscope and coherent light is passed longitudinally through the sample, as in Fig. 13 on the next page. When combined with a reference wave, the light forms an interference pattern, as illustrated in Fig. 14 on page 20. The interference fringes in the cladding material provide a reference line (and can be used to check the parallelness of the surfaces and the alignment of the instrument). The deflection, $S(r)$, of the interference fringe from the reference line at a radial position along the baseline, r , is measured and recorded. For an illumination wavelength, λ , a slab thickness, d , and a fringe spacing in the cladding of D , interference theory [1] predicts a refractive index profile given by

$$n(r) - n_2 = \frac{\lambda S(r)}{dD}. \quad (13)$$

The primary difficulty with this technique is the time and precision required in the preparation of the sample.

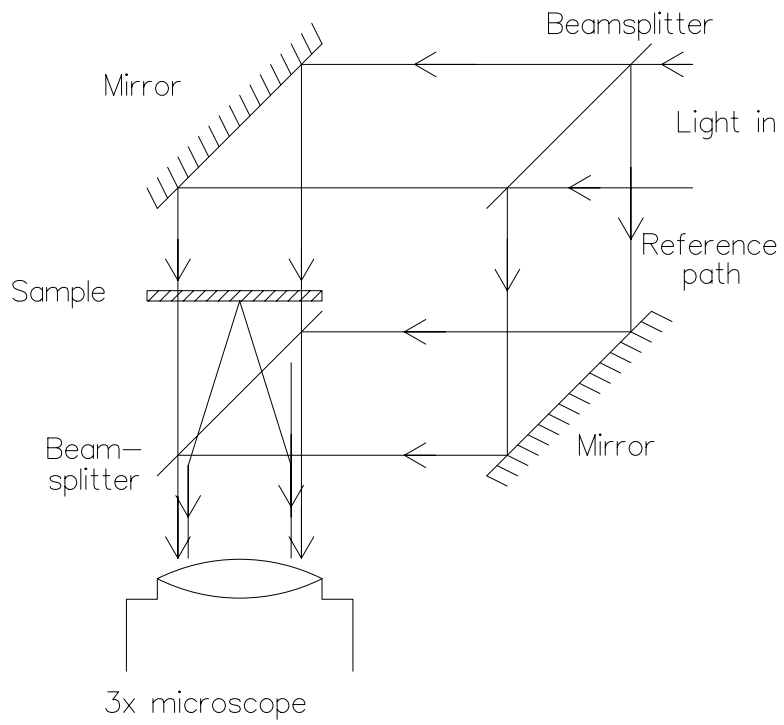


Figure 13: Setup for interference microscope.

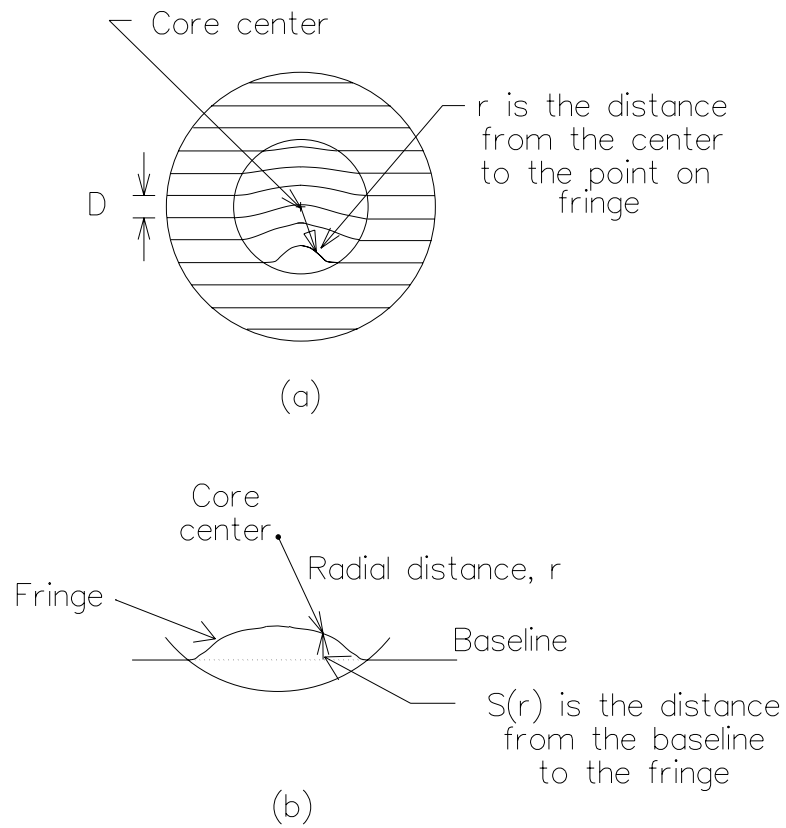


Figure 14: Geometry of interference pattern of the interferometric slab technique.

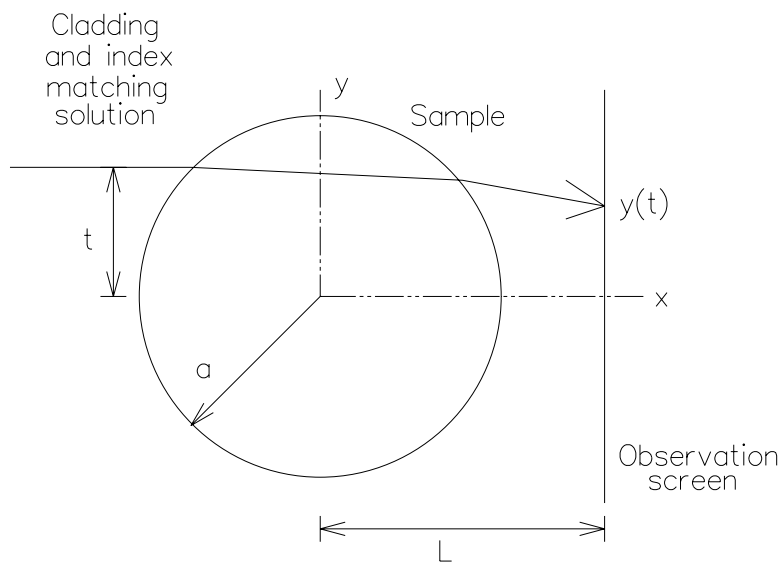


Figure 15: Geometry of the ray-tracing technique and the focusing method.

The second interference technique is the *transverse interferometric method* [39], which immerses the fiber in a liquid that matches the cladding index and illuminates the fiber (or preform) from the side with a coherent wave. After combining with a reference wave, the interference pattern is found. Using a computer-controlled pattern scanner, an integral equation can be solved by the computer to yield the refractive index profile. The advantage of this technique is its comparative speed, since minimal sample preparation is required.

8.5 Ray-Tracing Techniques [40]

Figure 15 illustrates the refraction of a light ray incident on an optical fiber or preform from the transverse direction (with the fiber immersed in an index matching solution with index n_2). Obviously, the deflection of the ray is dependent on Snell's Law at the interfaces and on the theory of propagation of rays in media with inhomogeneous velocities. For a circularly symmetric fiber, a ray entering at height, t , (as in Fig. 15) will appear at a screen a distance, L , away from the fiber at a height, $y(t)$, given by

$$y(t) = t + \frac{2Lt}{n_2} \int_t^a \frac{1}{\sqrt{r^2 - t^2}} \frac{\partial n(r)}{\partial r} dr. \quad (14)$$

With knowledge of $y(t)$, as measured by illuminating the sample with rays (i.e., pencil beams) at various values of t , the refractive index profile can be calculated as

$$n(r) - n_2 = \frac{n_2}{\pi L} \int_r^a \frac{t - y(t)}{\sqrt{t^2 - r^2}} dt. \quad (15)$$

The primary disadvantage of this method is the need to form the pencil beams and the sequential nature of the measurement. These disadvantages are overcome by the “focusing” method, discussed next.

8.6 Focusing Method [41, 42]

The *focusing method* was developed as an improved version of the ray-tracing technique that would illuminate the preform with a collimated beam, thereby producing all rays from the object simultaneously. The resulting image located a distance, L , is scanned in the y direction producing a power distribution, $P(y)$.

From this power distribution it is possible to deduce the corresponding entry ray height, $t(y)$, with the formula

$$t(y) = \int_0^y p(y') dy'. \quad (16)$$

In performing this integral on a computer, the results are pairs of values of y and t . Using these same sets of values with t as the independent variable and y as the dependent variable, the integral of Eq. 15 can be evaluated to find $n(r)$.

The method is fast and nondestructive. The region in the center is sensitive to error if there is a dip in the index of refraction, since the rays can cross each other before falling on the screen (in violation of the implicit assumptions that are made in using Equations 15 and 16). The overall shape of the index profile is accurately portrayed, but some errors are made in attempting to portray any ripple features in the profile. Cleanliness is required at the source, at the glass-liquid interface, and at the detector.

8.7 Diagnostigram Technique [40]

In this method, applied to preforms, a collimated beam of light (either coherent or incoherent) illuminates the sample transversely. Since the preform is a layered structure, there will be successive reflections and transmissions from the different layers. When intercepted on the far side of the sample on a ground glass screen, there is a pattern of (ideally) parallel lines in the preform image (called a *diagnostigram*). Each line in the pattern corresponds to a layer in the preform. As the preform is rotated, the image can be inspected for symmetry and the locations of defects can be noted qualitatively. The technique has been used to measure core size and ellipticity, to measure the core-cladding interface homogeneity, to inspect the uniformity of the layer structures, to detect the presence of an axial depression in the refractive index profile, and to locate

imperfections in the core and cladding. The method is rapid, real-time, nondestructive, and noncontacting.

9 Summary

In this chapter we have reviewed the fabrication of optical fibers by both high- and low-temperature techniques, the characterization of both preforms and fibers to measure their refractive index profile, and, finally, the techniques used to measure the operating performance of the optical fibers. The fabrication methods are dominated by the vapor-phase processes that ensure tight control over the purity of the deposition and the layer thicknesses. To measure the resulting preforms and fibers, a variety of ingenious techniques have been devised to meet the required measurement tolerances.

10 Problems

1. Using the principle of conservation of mass, calculate the approximate length of fiber that will be obtained from a 15 mm diameter preform that is 1 m long . . .
 - (a) . . . if the outside diameter (O.D.) of the fiber is 125 μm .
 - (b) . . . if the O.D. is 200 μm ?
2. Assume an ideal fiber drawing process.
 - (a) Calculate the diameter of a fiber drawn from a preform with an outside diameter of 12 mm moving with a 0.1 mm/s velocity if the fiber take-up velocity is 0.75 m/s?
 - (b) Find the velocity of the preform feed mechanism required to make a fiber with an outside diameter of 125 μm .
3. A silica tube with an inner diameter of 3 mm and an outer diameter of 4 mm is to be used in a MCVD process to make preform for a fiber with a 50 μm core diameter and an outside diameter of 125 μm .
 - (a) Calculate the thickness of the material that should be deposited inside this tube.
 - (b) Calculate the diameter of the core material and the diameter of the preform after the center hole has been removed.
 - (c) If this preform is to be used in a drawing machine that feeds in the preform at a rate of 1 cm/s, what should the fiber drawing speed be (assuming an ideal process)?
4. The interferometric-slab technique is used to measure the refractive index of a fiber. The fiber is found to have an index profile given by $n(r) = n_1[1 - \Delta(r/a)]$ (i.e., a triangular profile). Sketch the output from the interference microscope for this case.

References

- [1] K. Beales, C. Day, A. Dunn, and S. Partington, "Multicomponent glass fibers for optical communications," *Proc. IEEE*, vol. 68, no. 10, pp. 1191–1194, 1980.
- [2] W. G. French, R. E. Jaeger, J. B. MacChesney, S. R. Nagel, K. Nassau, and A. D. Pearson, "Fiber preform preparation," in *Optical Fiber Telecommunications* (S. E. Miller and A. G. Chynoweth, eds.), pp. 233–261, New York: Academic Press, 1979.
- [3] P. Shultz, "Progress in optical waveguide process and materials," *Applied Optics*, vol. 18, pp. 108–117, 1979.
- [4] J. MacChesney, "Materials and processes for preform fabrication — modified vapor deposition and plasma vapor deposition," *Proc. IEEE*, vol. 68, no. 10, pp. 1181–1184, 1980.
- [5] S. R. Nagel, "An overview of the modified chemical vapor deposition (MCVD) process and performance," *IEEE J. Quantum Electronics*, vol. QE-18, no. 4, pp. 459–476, 1982.
- [6] D. P. Jablonowski, "Fiber manufacture at AT&T with the MCVD process," *J. Lightwave Technology*, vol. LT-4, no. 8, pp. 1016–1019, 1986.
- [7] S. R. Nagel, "Fiber material and fabrication methods," in *Optical Fiber Telecommunications II* (S. E. Miller and I. P. Kaminow, eds.), pp. 121–215, New York: Academic Press, 1988.
- [8] H. Lydtin, "PCVD: A technique suitable for large-scale fabrication of optical fibers," *J. Lightwave Technology*, vol. LT-4, no. 8, pp. 1034–1038, 1986.
- [9] M. Blakenship and C. Denka, "The outside vapor deposition method of fabricating optical waveguide fibers," *IEEE J. Quantum Electronics*, vol. QE-18, no. 10, pp. 1418–1423, 1982.
- [10] R. V. Vandewoestine and A. J. Morrow, "Developments in optical waveguide fabrication by the outside vapor deposition process," *J. Lightwave Technology*, vol. LT-4, no. 8, pp. 1020–1025, 1986.
- [11] T. Izawa and N. Inagaki, "Materials and processes for fiber preform fabrication — vapor-phase axial deposition," *Proc. IEEE*, vol. 68, no. 10, pp. 1184–1187, 1980.
- [12] K. Inada, "Recent progress in fiber fabrication techniques by vapor-phase axial deposition," *IEEE J. Quantum Electronics*, vol. QE-18, no. 10, pp. 1424–1431, 1982.
- [13] H. Murata, "Recent developments in vapor phase axial deposition," *J. Lightwave Technology*, vol. LT-4, no. 8, pp. 1026–1033, 1986.
- [14] R. E. Jaeger, A. D. Pearson, J. C. Williams, and H. M. Presby, "Fiber drawing and control," in *Optical Fiber Telecommunications* (S. E. Miller and A. G. Chynoweth, eds.), pp. 263–298, New York: Academic Press, 1979.
- [15] L.L. Blyler, Jr. and F. DiMarco, "Fiber drawing, coating, and jacketing," *Proc. IEEE*, vol. 68, no. 10, pp. 1194–1198, 1980.
- [16] U. Paek, "High-speed high-strength fiber drawing," *J. Lightwave Technology*, vol. LT-4, no. 8, pp. 1048–1060, 1986.
- [17] Y. Hibino and H. Hanafusa, "Consolidation-atmosphere influence on drawing-induced defects in pure silica optical fibers," *J. Lightwave Technology*, vol. 6, no. 2, pp. 172–178, 1988.

-
- [18] Lee L. Blyler, Jr., B. R. Eichenbaum, and H. Schonhorn, "Coatings and jackets," in *Optical Fiber Telecommunications* (S. E. Miller and A. G. Chynoweth, eds.), pp. 299–341, New York: Academic Press, 1979.
- [19] J. Kreidl, "A surge in military demand for hermetic fiber," *Lightwave*, vol. 4, no. 11, p. 1, November 1987.
- [20] K. Lu, G. Glasemann, R. Vandewoestine, and G. Kar, "Recent developments in hermetically coated fiber," *J. Lightwave Technology*, vol. 6, no. 2, pp. 240–244, 1988.
- [21] C. B. Kurkjian, J. T. Krause, and M. J. Matthewson, "Strength and fatigue of silica optical fibers," *J. Lightwave Technology*, vol. 7, no. 9, pp. 1360–1370, 1989.
- [22] N. Yoshizawa, H. Tada, and Y. Katsuyama, "Strength improvement and fusion splicing for carbon-coated optical fiber," *J. Lightwave Technology*, vol. 9, no. 4, pp. 417–421, 1991.
- [23] C. Kurkjian and D. Inness, "Understanding mechanical properties of lightguides: a commentary," *Optical Engineering*, vol. 30, no. 6, pp. 681–689, 1991.
- [24] V. Bogatyryov, M. Bubnov, E. Dianov, S. Rumyantzev, and S. Semjonov, "Mechanical reliability of polymer-clad and hermetically coated fibers based on proof testing," *Optical Engineering*, vol. 30, no. 6, pp. 690–699, 1991.
- [25] D. Inness and J. Krause, "Hermetic splice overcoating," *Optical Engineering*, vol. 30, no. 5, pp. 776–779, 1991.
- [26] L. G. Cohen, P. Kaiser, P. D. Lazay, and H. M. Presby, "Fiber characterization," in *Optical Fiber Telecommunications* (S. E. Miller and A. G. Chynoweth, eds.), pp. 343–399, New York: Academic Press, 1979.
- [27] H. Presby and D. Marcuse, "Optical fiber preform diagnostics," *Applied Optics*, vol. 18, no. 11, pp. 23–30, 1979.
- [28] C. Saekang, P. Chu, and T. Whitbread, "Nondestructive measurements of refractive-index profile and cross-sectional geometry of optical fiber preforms," *Applied Optics*, vol. 19, no. 2, pp. 2025–2030, 1980.
- [29] P.-L. Francois, I. Sasaki, and M. Adams, "Practical three-dimensional profiling of optical fibers," *IEEE J. Quantum Electronics*, vol. QE-18, no. 4, pp. 524–535, 1982.
- [30] W. Stewart, "Optical fiber and preform profiling technology," *IEEE J. Quantum Electronics*, vol. QE-18, no. 10, pp. 1451–1466, 1982.
- [31] K. Morishita, "Index profiling of three-dimensional optical waveguides by the propagation-mode near-field technique," *J. Lightwave Technology*, vol. LT-4, no. 8, pp. 1120–1124, 1986.
- [32] K. Raine, J. Barnes, and D. Putland, "Refractive index profiling — State of the art," *J. Lightwave Technology*, vol. 7, no. 8, pp. 1162–1169, 1989.
- [33] J. Helms, J. Schmidtchen, B. Schüppert, and K. Petermann, "Error analysis for refractive-index profile determination from near-field measurements," *J. Lightwave Technology*, vol. 8, no. 5, pp. 625–633, 1990.
- [34] F. P. Kapron, "Fiber-optic test methods," in *Fiber Optics Handbook for Engineers and Scientists* (F. C. Allard, ed.), pp. 4.1–4.54, New York: McGraw-Hill, 1990.

- [35] D. Marcuse, D. Gloge, and E. A. Marcatili, "Guiding properties of fibers," in *Optical Fiber Telecommunications* (S. E. Miller and A. G. Chynoweth, eds.), pp. 37–100, New York: Academic Press, 1979.
- [36] A. H. Cherin, *Introduction to Optical Fibers*. New York: McGraw-Hill, 1983.
- [37] J. Senior, *Optical Fiber Communications: Principles and Practice*. Englewood Cliffs, NJ: Prentice Hall, 1985.
- [38] M. Saunders, "Nondestructive interferometric measurement of the delta and alpha of optical fibers," *Applied Optics*, vol. 16, no. 9, pp. 2368–2371, 1977.
- [39] K. Iga and Y. Kokobun, "Formulas for calculating the refractive index profile of optical fibers from their transverse interference patterns," *Applied Optics*, vol. 17, no. 12, pp. 1972–1974, 1978.
- [40] H. Presby and D. Marcuse, "The index–profile characterization of fiber preforms and drawn fibers," *Proc. IEEE*, vol. 68, no. 10, pp. 1198–1203, 1980.
- [41] D. Marcuse and H. Presby, "Effects of profile deformations on fiber bandwidth," *Applied Optics*, vol. 18, pp. 3758–3763, 1979.
- [42] D. Marcuse, "Refractive index determination by the focusing method," *Applied Optics*, vol. 18, no. 1, pp. 9–13, 1979.
- [43] M. Schwartz, P. Gagen, and M. Santana, "Fiber cable design and characterization," *Proc. IEEE*, vol. 68, no. 10, pp. 1214–1219, 1980.
- [44] S. Foord, "Fibre–optic cables," in *Optical Fibre Communication Systems* (C. Sandbank, ed.), pp. 70–85, New York: Wiley, 1980.
- [45] T. Nakahara and N. Uchida, "Optical cable design and characterization in Japan," *Proc. IEEE*, vol. 68, no. 10, pp. 1220–1226, 1980.
- [46] J. E. Goell, "Optical fiber cable," in *Fundamentals of Optical Fiber Communications* (M. F. Barnoski, ed.), pp. 109–146, New York: Academic Press, 1981.
- [47] P. Kaiser and W. T. Anderson, "Fiber cables for public communications: State-of-the-art technologies and the future," *J. Lightwave Technology*, vol. LT-4, no. 8, pp. 1157–1166, 1986.
- [48] Charles H. Gartside III, P. D. Patel, and M. R. Santana, "Optical fiber cables," in *Optical Fiber Telecommunications II* (S. E. Miller and I. P. Kaminow, eds.), pp. 217–261, New York: Academic Press, 1988.
- [49] M. M. Ramsay, "Fiber-optic cables," in *Fiber Optics Handbook for Engineers and Scientists* (F. C. Allard, ed.), pp. 2.1–2.50, New York: McGraw-Hill, 1990.